JOURNAL OF MATERIALS SCIENCE 29 (1994) 91–98

The effect of the loading rate on the fracture toughness of Poly(methyl methacrylate), Polyacetal, Polyetheretherketone and modified PVC

PH. BEGUELIN, H. H. KAUSCH
Ecole Polytechnique Fédérale de Lausanne, MX-D 1015 Lausanne, Switzerland

The mode-I-plane-strain fracture toughness at initiation of various engineering plastics was determined for test speeds between 10^{-4} m s^{-1} and 10 m s^{-1}, using a high-speed, servohydraulic testing apparatus. At high rates of testing, the transient acceleration of the specimen was reduced by the use of a damping technique aimed at overcoming dynamic effects. The results obtained are correlated with fractographic analysis performed by scanning electron microscopy (SEM) and by digital image analysis of macroscopic fracture surfaces. The results show that for some materials the high values of K_{Ic} measured at low testing rates are associated with deformation detectable by either method. The extent of such deformation tends to be reduced as the testing velocity is increased and the fracture toughness drops.

1. Introduction

There is increasing interest in the behaviour of polymers at high deformation rates and under impact-loading conditions. For many years, impact resistance has been measured by Charpy and Izod tests. More recently the fracture-mechanics approach has been used for three-point-bending impact [1]. Fracture-mechanics analysis is available for various test geometries, and is based on load or displacement measurements when fracture occurs. However, the force recorded by a transducer located in the striker of an instrumented pendulum or drop-weight carriage is difficult to interpret at high rates of testing because of problems in identifying the onset of fracture, particularly when the specimen is brittle.

At high testing rates, inertial forces due to the rapid acceleration of the specimen interact with the external applied stress [2]. Thus, the acceleration of the tested specimen depends on the velocity of the striker, the apparent stiffness of the specimen, and on the contact stiffness [3, 4]. A model has been proposed [4, 5] which shows that, for short times to fracture, measurements must be made on the specimen itself. The best results have been obtained through the measurement of the time to fracture by means of a crack-propagation gauge. The fracture-mechanics analysis is then based on the force [6] or the specimen deflection [7] at the moment of fracture.

The use of several test methods to cover a wide range of testing velocities often fails to provide consistent data. Moreover, results from different types of impact tests do not correlate [8]. For a better understanding of the effect of loading rates on polymer deformation and fracture it is desirable that the same test can be performed over a wide range of testing velocities. This means that the dynamic effects occurring at high testing speeds have to be corrected when a force transducer external to the sample is used. A promising method uses experimental dynamic calibration curves established by means of the shadow optical method of caustics and high-speed photography [9].

In contrast to conventional impact-test methods, the testing procedure described here is designed to provide a high loading rate at the crack tip of prenotched specimens at a high testing speed, while reducing their transient acceleration by means of a viscoelastic damper. Consequently, this method provides continuous fracture-toughness measurements at initiation from low loading rates up to loading rates of the order of magnitude of those reached in impact testing.

This paper reports the plane strain fracture toughness measured at room temperature in Poly(methyl methacrylate) (PMMA), Polyacetal (POM), Polyetheretherketone (PEEK), and modified Poly (vinyl chloride) (mPVC) at testing velocities from 10^{-4} to 10 m s^{-1}. The results are correlated with fractographic studies using scanning electron microscopy (SEM). For the mPVC, the correlation is made with macroscopic whitening of the fractured surfaces.

2. Experimental procedure

2.1. Test geometry

Among the various specimen geometries used in fracture mechanics, compact tension (CT) specimens were chosen because the specimen is held by means of pins,

0022–2461

avoiding loss of contact between the specimen and adjacent transducers (force and displacement).

In order to reduce the weight of the fixing parts, the standard CT geometry has been slightly modified by the machining of a vertical slit on the precracked side of the specimens, as shown in Fig. 1.

2.2. Materials

Details of the four materials tested are summarized in Table I. In the case of PMMA, POM and PEEK, the notch was machined, and then natural precracks of different lengths, a, were introduced by tapping a razor blade in the notch at ambient temperature. The precracking of mPVC was performed on specimens just after removal from storage at $-18\,^{\circ}C$.

2.3. Testing equipment and dynamic effects

Testing was performed on a servohydraulic, high-speed, testing machine manufactured by Schenck. These machines operate like any other standard hydraulic testers for velocities up to approximately $0.5\,m\,s^{-1}$. For higher velocities, owing to its high mass, the piston rod has to be accelerated freely, without strain being induced in the specimen during the acceleration process. Once the piston has reached the desired velocity, the motion is transmitted to the specimen by a mechanical assembly referred to here as the pick-up unit (Fig. 2).

It has been shown that the nature of the contact in the pick-up dramatically influences the resulting strain rate [10, 11]. A high contact stiffness produces a high transient acceleration in the sample fixture. As a result, the velocity applied to the specimen oscillates, with an initial value higher than that of the piston rod. The loading rate at a given piston speed depends on the stiffness of the materials at the surfaces of contact, the compliance of the specimen and the masses of the mechanical fixtures. The forces measured by an external transducer or by strain gauges fixed on the specimen also oscillate.

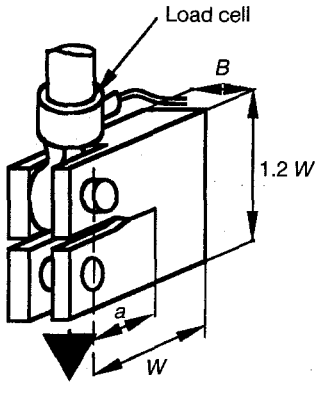

Figure 1 Modified compact tension (CT) test geometry. $W = 20$ mm.

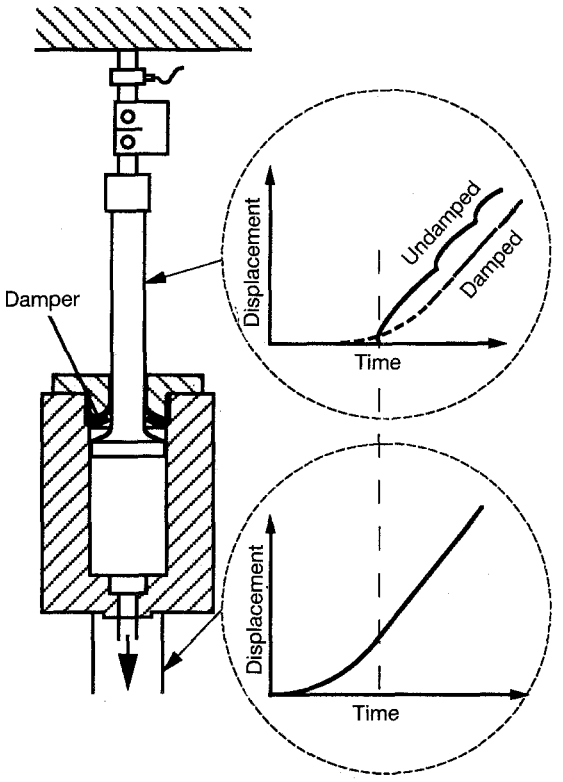

Figure 2 Mechanical design of the pick-up unit and displacement profiles.

Damping the contact in the pick-up unit with a viscoelastic rubber-like material, having a low coefficient of restitution, will significantly decrease the acceleration of the specimen. The use of such a material extends the range in which inertial forces can be neglected. The material used in this study was a filled polyurethane elastomer, with a low cross-linking density (Viscolas, Chattanogga Corporation), selected for its excellent damping properties. This procedure has been used in previous work to study the tensile and delamination properties of PEEK [10].

A load cell having a low mass (6.5 g) was constructed from titanium, starting from a piezoelectric load ring. The resonant frequency of this cell, including the pin fixture is 65 kHz. It was attached to the stationary end of the specimen.

TABLE I Details of the materials used

Polymer		Designation	Producer	Manufacturing process	Thickness, B
PMMA	Poly(methyl methacrylate)	233	Röhm	Casting	10.1 mm
POM	Polyacetal	Delrin 500	Du Pont	Compression moulding	10.2 mm
PEEK	Polyetheretherketone	450 G	ICI	Injection moulding	~ 12 mm
mPVC	Poly(vinyl chloride) modified with 4 % chlorinated polyethylene	Pipe grade to BS3505	EVC	Cut from extruded pipes, plaques reheated at 120 °C, cooled between steel plates	8.5 mm

The true opening of the moving fixture was measured with an optical device. A laser light beam was injected into a thin optical fibre (250 μm external diameter); the free end of the optical fibre was attached to the moving part and it acted as a light emitter. The position of this light was detected by a linear optical detector aligned with the emitter. This method provided accurate position measurement of the moving parts, for both undamped and damped testing procedures.

For certain experiments, such as those shown in Fig. 3, the crack position was measured by means of a graphite gauge [12].

The data acquisition was made with a transient memory recorder capable of performing A/D sampling at rates up to 2×10^6 samples s^{-1}. The data were analysed on a HP340 computer.

3. Measurements and analysis

To compare the effects of damped and undamped loading, Fig. 3 shows the recordings of force, displacement and crack length made with POM specimens. When the contact in the pick-up unit was unmodified (steel on titanium), the measured force exhibited several peaks as shown in Fig. 3a; the unstable crack propagation recorded by the graphite gauge does not coincide with the maximum force. This is typical of the dynamic situation, where the specimen and the load cell were excited at their resonance frequencies by the transient acceleration resulting from a high contact stiffness. Even when the exact time of the onset of fracture was known, the readings of the force at this time were meaningless.

The effect of damping the contact in the pick-up unit was to substantially reduce the initial acceleration induced in the specimen and the attached force transducer. The effect on the measured force is shown in Fig. 3b: the force has a single peak that corresponds to the onset of unstable fracture. We believe that this damped procedure results in a quasistatic stress-state condition at the crack tip for the whole duration of the test.

Note that the 13 μs time shift occurring between the detection of the fracture by the crack gauge and the rapid drop in the force is due to the time for the waves to travel from the crack front, where the crack gauge is located, to the load transducer, some 15 mm away. As the crack gauge was applied after the precracking of the specimens, the crack propagation measured during the loading phase, before unstable fracture, resulted from the cracking of the part of the gauge covering the precrack.

Compared with the undamped procedure, the time to fracture in a damped test is larger, but this does not seem to affect the values measured. Tests performed using both the damped and undamped methods, at crack-tip loading rates between 100 and 5000 MPa $m^{1/2}$ s^{-1} show similar results and fracture surfaces. Similar observations have been made by Mills and Zhang on PS tested under impact loading [13].

A conventional force-based analysis has been used to determine the fracture toughness K_I [1]. The critical stress-intensity factor at initiation K_{Ic} has been calculated from the maximum force measured using the damped procedure.

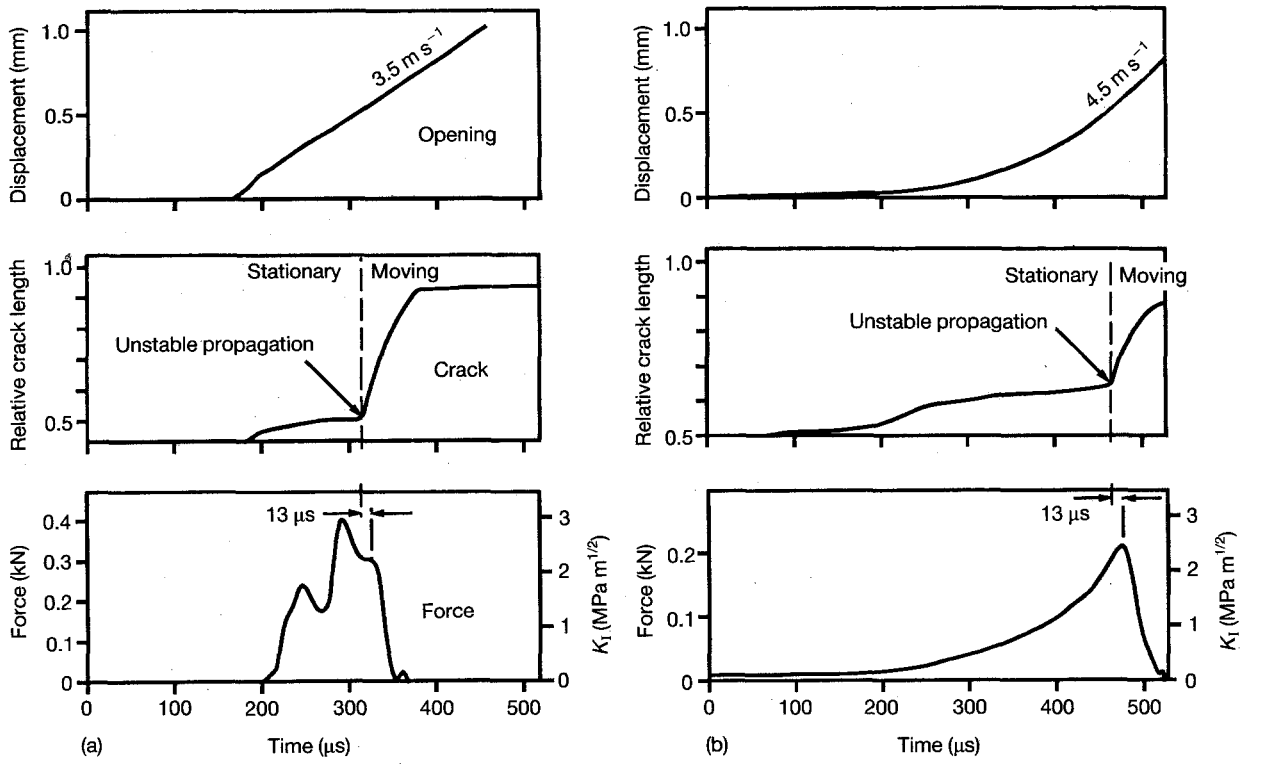

Figure 3 Influence of the nature of the contact in the pick-up unit on the displacement rate and on the loading-time curve measured on POM: (a) undamped contact, and (b) damped contact.

The loading situation has been characterized using the crack-tip loading rate $\dot{K}$. It is calculated from the gradient, $\dot{P}$, of the force-against-time graph measured just before propagation.

$$K_{Ic} = f\frac{P_c}{BW^{1/2}}, \quad \frac{dK}{dt} = \dot{K} = f\frac{\dot{P}}{BW^{1/2}}$$

where f is a calibration factor dependent on the geometry and crack length, P_c is the load measured at propagation, B is the thickness and W is the depth of the specimen.

The tests were conducted at room temperature. PMMA, POM and PEEK were tested at piston velocities from 10^4 m s^{-1} to 10 m s^{-1}. Because of the high, macroscopic, shear deformation at low velocities, the mPVC was tested from 8×10^{-1} m s^{-1} to 10 m s^{-1}.

4. Results

The interest in plotting the stress-intensity factor, K_{Ic}, versus the crack-tip loading rate is that the only measured variables required are force and time. Thus any change in strain rate at the crack tip between samples with different precrack lengths is corrected by the change in compliance.

Fig. 4 shows such a plot for high-molecular-weight PMMA. Totally or partially stable crack propagation occurred at the lower velocities and is represented by the filled squares. At higher opening velocities, the crack propagation was always unstable. The fracture toughness remained constant over the whole range of crack-tip loading rates, as shown by the linear regression analysis (solid line in Fig. 4).

A similar plot for POM, Fig. 5, shows a moderate decrease of the fracture toughness when the loading rate was increased.

The notch sensitivity of PEEK to the loading rate is high, as shown in Fig. 6. The drop in fracture toughness with increasing loading rate is considerable, but is found to occur at higher velocities than those measured by Karger-Kocsis and Friedrich [14].

The results obtained with these three materials have been combined in Fig. 7. The top scale in this diagram indicates the testing velocity.

The toughness of the mPVC also appears to be highly rate dependent. As shown in Fig. 8, the scatter of the results is large and will be discussed later.

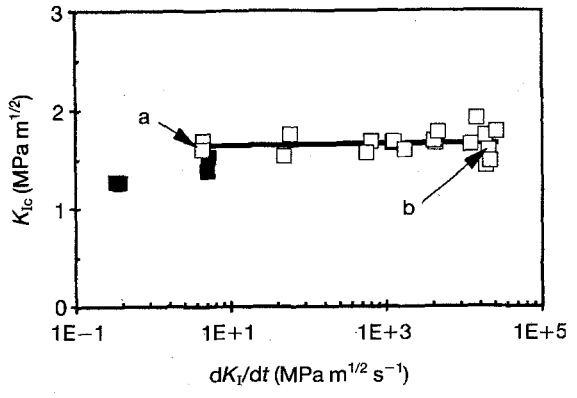

Figure 4 Loading-rate effect on PMMA: (■) stable crack propagation, and (□) unstable crack propagtion (a and b refer to Fig. 9).

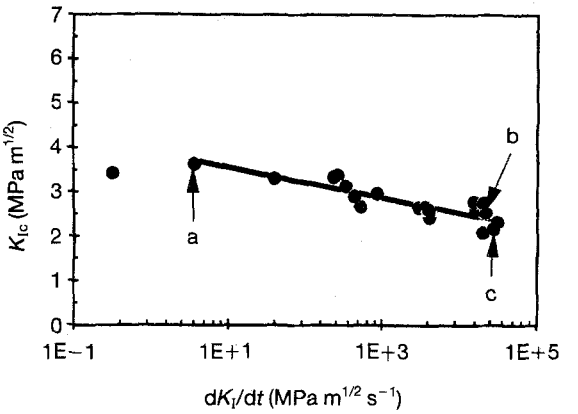

Figure 5 Loading rate effect on POM (a, b and c refer to Fig. 10).

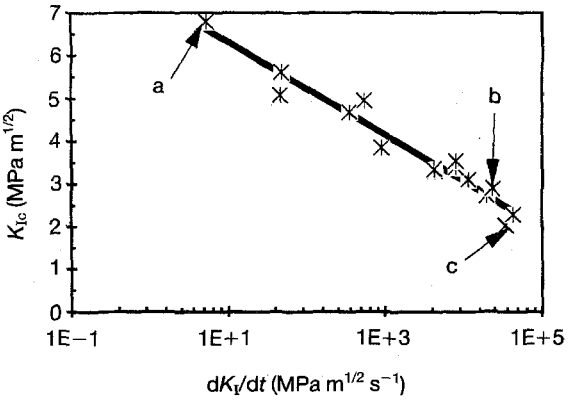

Figure 6 Loading-rate effect on PEEK (a, b and c refer to Fig. 11).

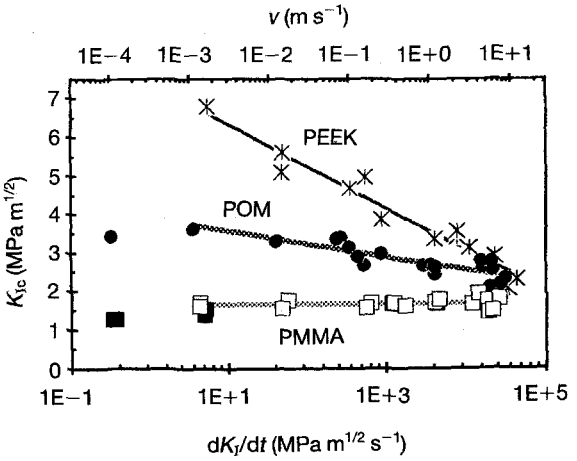

Figure 7 Comparison of the effect of the loading rate on PMMA, POM and PEEK. The top scale indicates the approximate testing speed.

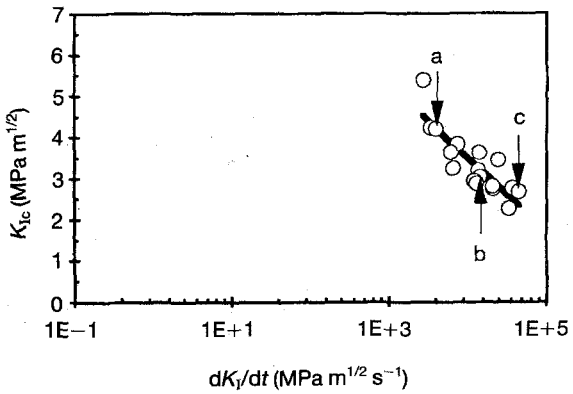

Figure 8 The effect of loading rate on PVC modified with chlorinated polyethylene (PE). (a, b and c refer to Fig. 15.)

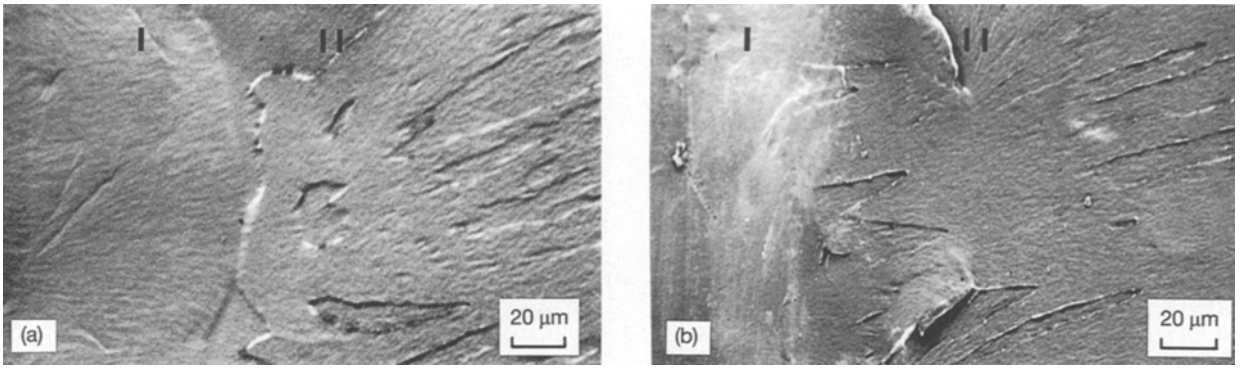

Figure 9 SEM fractography of PMMA tested at: (a) 10^{-3} m s^{-1} and K_{Ic} = 1.4 MPa m$^{1/2}$, and (b) 9.6 m s^{-1} and K_{Ic} = 1.5 MPa m$^{1/2}$. I is the precrack zone and II is the unstable-crack-propagation zone.

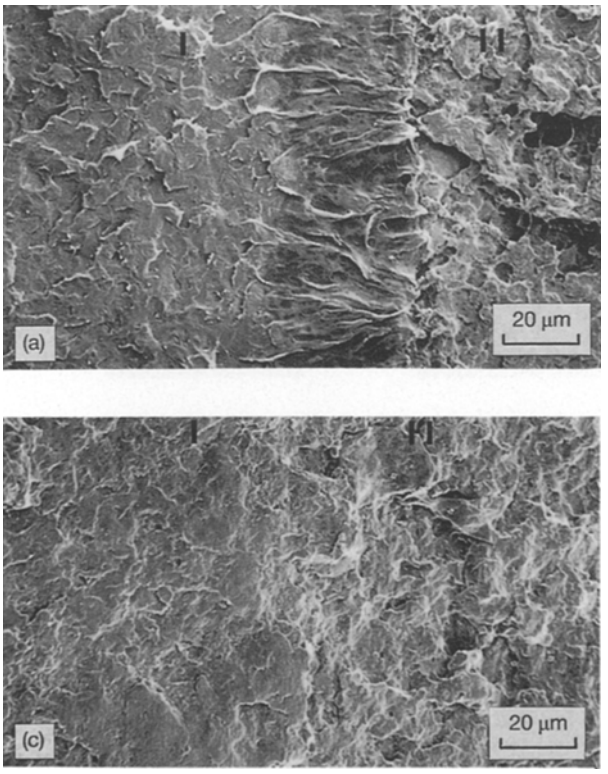

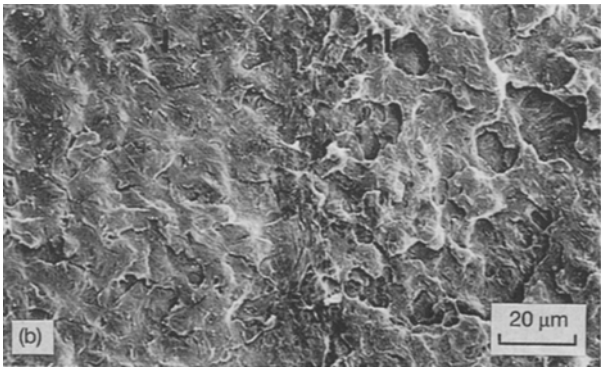

Figure 10 SEM fractography of POM tested at: (a) 10^{-3} m s^{-1} and K_{Ic} = 3.6 MPa m$^{1/2}$, (b) 6 m s^{-1} and K_{Ic} = 2.75 MPa m$^{1/2}$, and (c) 10 m s^{-1} and K_{Ic} = 2.03 MPa m$^{1/2}$. I is the precrack zone and II is the unstable-crack-propagation zone.

5. Fractographic observations

We used SEM to study the fracture-surface topology just in front of the precrack of specimens fractured at different opening velocities. The particular specimens examined are identified in Figs 4–6 and 8.

Zone I of the micrographs corresponds to the fracture area occurring in front of the razor blade during the prenotching operation. Zone II is the fracture surface resulting from the fast crack growth initiated in the test. The region of interest is located between zone I and II, since it is expected to be the process zone prior to unstable crack propagation. Any possible changes in the deformation mechanism such as crack blunting or single or multiple crazing resulting from the time-related loading process are expected to occur in this region.

5.1. PMMA

The fracture surfaces are relatively smooth and the textures marking the early stages of the unstable crack-propagation zone developed at the testing speed of 10^{-3} m s^{-1} (Fig. 9a) are similar in size and shape to those found at nearly 10 m s^{-1} (Fig. 9b). No obvious change in the deformation mechanism was observed.

5.2. POM

The observation of the specimen tested at an opening velocity of 10^{-3} m s^{-1} clearly shows a zone of microscopic yielding in the early stages of crack growth (Fig. 10a). Whether this deformation is initiated in the amorphous intercrystalline regions, which are above T_g at room temperature, is not yet clear. When the testing speed increases (6 m s^{-1}) this zone becomes less distinct (Fig. 10b). At this scale of magnification, it disappears at 10 m s^{-1}, as shown in Fig. 10c.

5.3. PEEK

The fractographic analyses of PEEK provide interesting observations of the presence of small scale yielding in front of the precrack.

At low loading rates, relatively large-scale yielding occurs. It is associated with significant non-linearity in

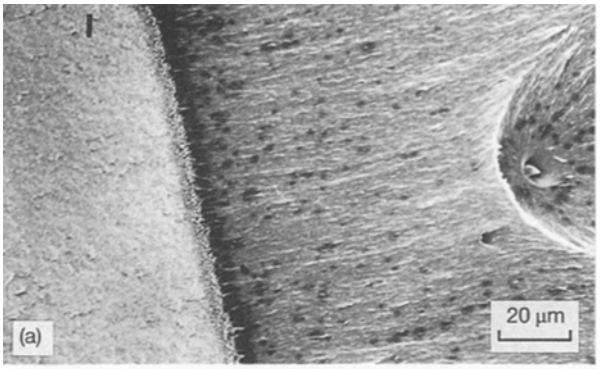

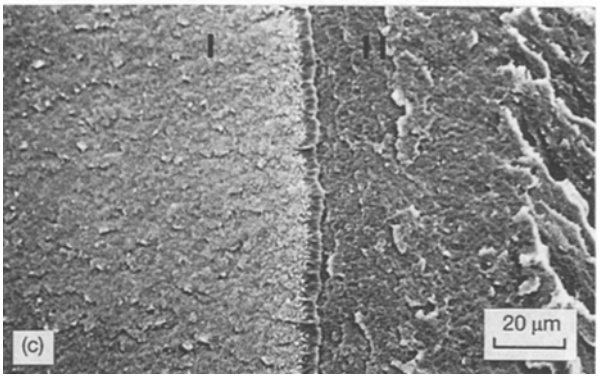

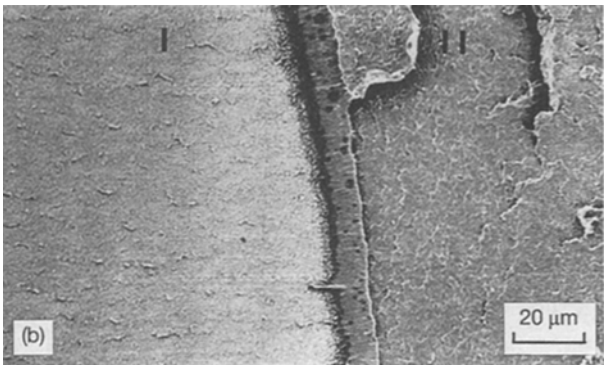

Figure 11 SEM fractography of PEEK tested at: (a) 10^{-3} m s^{-1} and K_{Ic} = 6.6 MPa m$^{1/2}$, (b) 5.3 m s^{-1} and K_{Ic} = 2.95 MPa m$^{1/2}$, and (c) 9.2 m s^{-1} and K_{Ic} = 2.01 MPa m$^{1/2}$. I is the precrack zone and II is the unstable-crack-propagation zone.

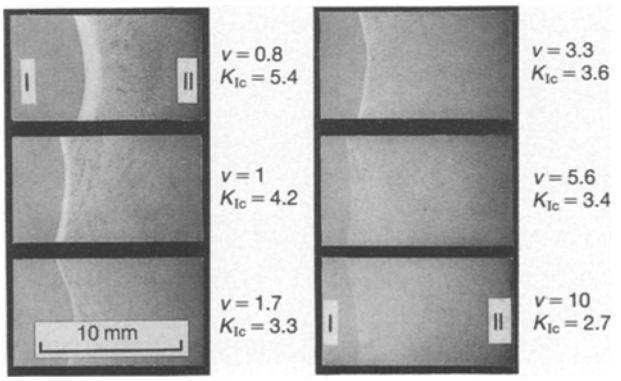

Figure 13 Evolution of the macroscopic stress whitening on the fracture surface of mPVC specimens tested at velocities, v, from 0.8 to 10 m s^{-1}.

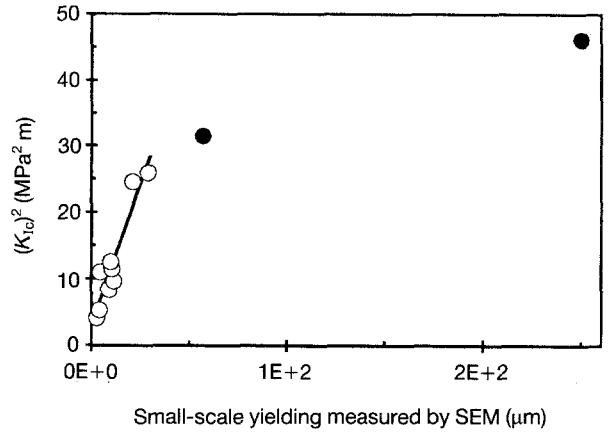

Figure 12 Square of the fracture toughness versus the length of the yield zone in PEEK measured by SEM: (●) the yield zone including parabolic features, and (○) non-parabolic features.

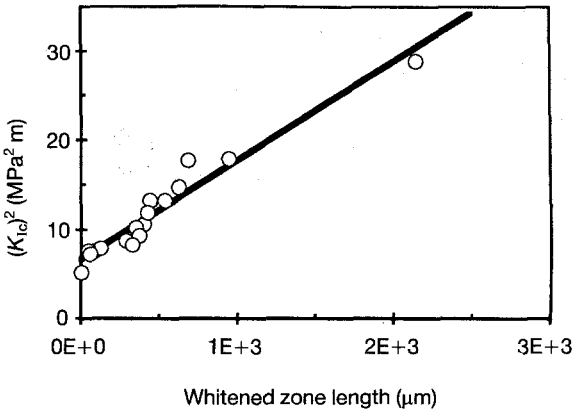

Figure 14 Square of the fracture toughness versus the normalized whitened zone measured in mPVC by image analysis.

the load–displacement curve. From this there is no evidence of stable crack growth prior to fast fracture. On the right-hand-side of Fig. 11a there is a highly deformed zone, which continues beyond the margin of the micrograph, developed in a specimen fractured at 10^{-3} m s^{-1}. This zone includes a parabolic feature centred on an inclusion. Similar observations have been reported following low-loading-rate experiments [15].

Fig. 11b and c reveals the strong dependence of the size of the zone of microyielding on the loading rate. The length of this zone was measured by SEM on 11 specimens fractured at different testing rates and is plotted in Fig. 12. Fig. 12 shows clearly a relationship between the fracture toughness and the scale of microscopic yielding. The values plotted were measured at the centre of the crack profile, where fully plane-strain conditions occur. This relationship appears to be linear with $(K_{Ic})^2$ for the low values of toughness corresponding to high testing velocities. The length of the zone is somewhat extended at velocities where parabolic patterns such as that shown in Fig. 11a occur.

The fibrillar structure along the left-hand side of the yield zone is believed to be produced during the arresting phase of the prenotch. This would explain why the size of this zone does not depend on the opening rate. This fibrillation has also been observed at the intermediate-to-fast propagation interface and

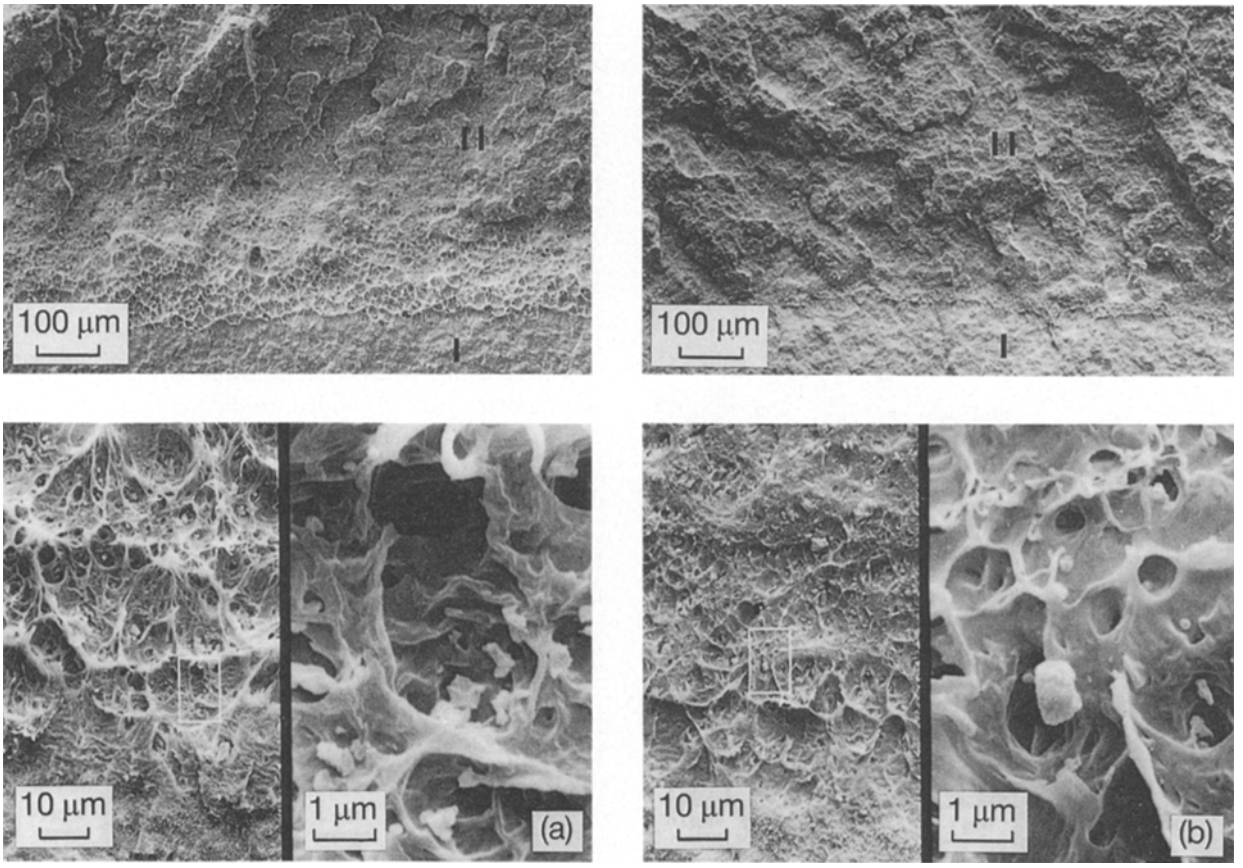

Figure 15 SEM fractography of mPVC tested at: (a) $1\,m\,s^{-1}$ and $K_{Ic} = 4.2\,MPa\,m^{1/2}$, and (b) $3.3\,m\,s^{-1}$ and $K_{Ic} = 3.1\,MPa\,m^{1/2}$, and (c) $10\,m\,s^{-1}$ and $K_{Ic} = 2.7\,MPa\,m^{1/2}$. I is the precrack zone and II is the unstable-crack-propagation zone.

has been attributed to the rupture of craze fibrils [16], although the scale of the fibrillar texture is up to two orders of magnitude greater than is normally observed by transmission electron microscopy (TEM) in glassy polymers. Similar fibrillar structures, have also been described as resulting from "nucleus pull-out" [15].

5.4. Modified PVC

This material, which is blue in the undeformed state, exhibits significant macroscopic stress whitening effect when subject to plastic deformation. Fig. 13 shows some examples of the fracture surfaces of broken specimens tested at different rates. A numerical image of each fracture surface has been taken with a video camera under identical lighting conditions, and transferred to a computer. Using an image-processing package (Optilab), a binary image was obtained at a constant threshold. The surface of white pixels (normalized by the specimen thickness) is plotted against the square of the fracture toughness, measured at different loading rates, in Fig. 14. These results clearly show a linear relationship between these two parameters.

SEM observations near the precrack of the specimens fractured at opening velocities from 1 to $10\,m\,s^{-1}$ are shown in Fig. 15. The macroscopic whitening resulting from small-scale yielding induced by the modifying particles is concentrated ahead of the prenotch (zone I). The size of these regions, in which most of the plastic deformation occurs, decreases with increasing testing velocity.The upper parts of the low-magnification micrographs correspond to unstable fracture of the specimens (Zone II). The intermediate magnifications reveal similar deformation mechanisms, but the matrix drawing around the particles is reduced when the time for yielding decreases at high

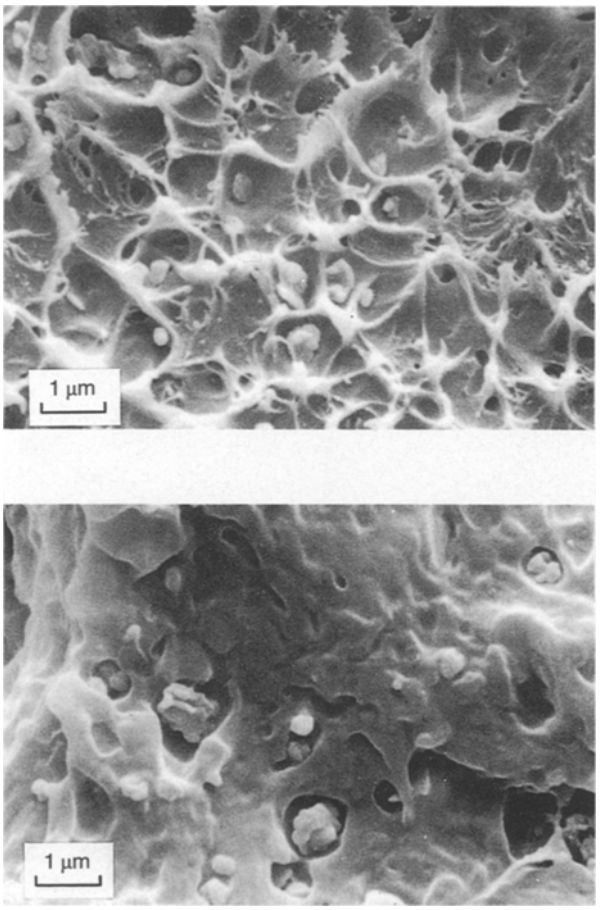

Figure 16 SEM observations of mPVC fractured at 10 m s^{-1} and K_{Ic} = 2.7 MPa m$^{1/2}$: top, process zone; and bottom, unstable-crack-propagation region.

testing rates. The higher magnifications show unchanged debonding and cavitational features around the particles at different testing rates.

The small-scale yielding appears to be strongly promoted by the presence of the modifier particles, and parameters such as modifier concentration and particle size in the process zone can affect the scatter in the measurement of the fracture toughness. Nevertheless, the correlation between the measured toughness and the small-scale yielding process (whitening) is good, as shown in Fig. 14.

A low value of fracture energy at room temperature might reasonably be expected when the deformation around the toughening particles in the process zone is small, i.e. if it does not exceed the value observed on the unstable fracture surface created by a crack running at several hundred of meters per second. The upper part of Fig. 16 shows quite-well-developed, small-scale plastic deformation around the particles in the process zone of a specimen fractured at 10 m s^{-1}. For comparison the lower part shows the much smoother fracture surface resulting from unstable crack propagation in the same specimen. This suggests that fracture-toughness values lower than those found at our highest testing velocities ($\sim$ 10 m s^{-1}), might be found at still higher velocities.

6. Conclusion

The test method applied here may be seen as an extension of the usual low-rate testing of materials, since it uses the same variables. The strain rates were increased, but the dynamic effects were reduced by means of a damper that reduced the transient acceleration of the specimen. In this way resonance of the specimen and the load cell was avoided. This approach permitted the measurement of fracture-mechanics parameters from low to intermediate loading rates.

The toughness measured for three of the four materials reported here depended on the loading rate. Only PMMA was unaffected by the loading rate, although a transition from stable to unstable crack propagation eventually occurred.

The K_{Ic} of PEEK and toughened PVC was found to be highly rate dependent. For these materials the drop in properties is associated with a reduction in the size of the plastic deformation involved in the fracture-initiation process.

In the loading range studied, none of the deformation mechanisms observed seemed to be affected by the occurrence of adiabatic heating prior to fracture initiation.

References

1. J. G. WILLIAMS, in "Fracture mechanics of polymers" (Ellis Horwood–Wiley, Chichester, 1984).
2. W. BÖHME and J. F. KALTHOFF, *J. Physique, Colloque C5, Supplément No 8* **46** (1985) 213–218.
3. C. ZANICHELLI, M. RINK, A. PAVAN and T. RICCO, *Polym. Engng. Sci.* **30** (1990) 1117–1124.
4. J. G. WILLIAMS, in Proceedings of the International Seminar on Impact Fracture of Polymers, Fukuoka, Japan, July 1991, edited by K. TAKAHASHI and A. F. YEE (Kyushu University Press, 1992) p. 393–423.
5. J. G. WILLIAMS and G. C. ADAMS, *Int. J. Fracture* **33** (1987) 209–222.
6. A. J. KINLOCH, G. A. KODOKIAN and M. B. JAMARANI, *J. Mater. Sci.* **22** (1987) 4111–4119.
7. G. C. ADAMS, R. G. BENDER, B. A. CROUCH and J. G. WILLIAMS, *Polym. Engng. Sci.* **30** (1990) 241–248.
8. S. N. KAKARALA and J. L. ROCHE, in "Instrumented impact of plastics and composites materials", ASTM STP 936 (American Society for the Testing of Materials, Houston, 1987) 144–162.
9. W. BÖHME, in "Fracture mechanics: twenty-first symposium", ASTM STP 1074 (American Society for the Testing of Materials, 1990) 144–156.
10. PH. BÉGUELIN, and M. BARBEZAT, *J. Physique III France* **1** (1991) 1867–1880.
11. PH. BÉGUELIN, in Proceedings of the International Seminar on Impact Fracture of Polymers, Fukuoka Japan, July 1991, edited by K. TAKAHASHI and A. F. YEE (Kyushu University Press, 1992) p. 291–302.
12. B. STALDER, PH. BÉGUELIN, A. C. ROULIN-MOLONEY and H. H. KAUSCH, *J. Mater. Sci.* **24** (1989) 2262–2274.
13. N. J. MILLS and P. S. ZHANG, *ibid.* **24** (1989) 2099–2109.
14. J. KARGER-KOCSIS and K. FRIEDRICH, *Polymer* **27** (1986) 1753–1760.
15. J-N. CHU and J. M. SCHULTZ, *J. Mater. Sci.* **24** (1989) 4538–4544.
16. D. PURSLOW, *Composites* **18** (1987) 365–374.

Received 15 June 1992
and accepted 20 April 1993